nature neuroscience

Hedgehog signaling promotes basal progenitor expansion and the growth and folding of the neocortex

Lei Wang[1,2], Shirui Hou[1,2] & Young-Goo Han[1,2]

The unique mental abilities of humans are rooted in the immensely expanded and folded neocortex, which reflects the expansion of neural progenitors, especially basal progenitors including basal radial glia (bRGs) and intermediate progenitor cells (IPCs). We found that constitutively active Sonic hedgehog (Shh) signaling expanded bRGs and IPCs and induced folding in the otherwise smooth mouse neocortex, whereas the loss of Shh signaling decreased the number of bRGs and IPCs and the size of the neocortex. SHH signaling was strongly active in the human fetal neocortex but Shh signaling was not strongly active in the mouse embryonic neocortex, and blocking SHH signaling in human cerebral organoids decreased the number of bRGs. Mechanistically, Shh signaling increased the initial generation and self-renewal of bRGs and IPC proliferation in mice and the initial generation of bRGs in human cerebral organoids. Thus, robust SHH signaling in the human fetal neocortex may contribute to bRG and IPC expansion and neocortical growth and folding.

The neocortex, a six-layered structure covering mammalian brains, computes high-order sensory, motor and cognitive processes. During evolution, the neocortex expanded dramatically and folded in certain species. The immense expansion of the neocortex in humans has made possible the complex behavior, cognition and intellect that are quintessential to humans. Neocortical expansion and folding reflect an increase in the number of neurons, especially upper-layer neurons, and are thus dependent on the number and proliferative capacity of neural progenitors[1–5]. The primary neural progenitors are radial glia, whose cell bodies reside in the ventricular zone at the apical side of the developing brain and are hence called ventricular radial glia (vRGs) or apical radial glia (aRGs). The aRGs generate neurons directly or via IPCs that occupy the subventricular zone (SVZ). Newborn neurons migrate along radial processes of radial glia through the intermediate zone to the cortical plate to form neuronal layers.

A neurogenic area basal to the archetypal SVZ was recently identified in the brains of monkeys and humans[6,7]. This area is called the outer SVZ (oSVZ) and is thought to be responsible for the expansion of the neocortex, especially the upper-layer neurons, in primates[6,8]. The primary neural progenitors in the oSVZ are outer radial glia (also called bRGs) that are detached from the ventricle but maintain some aRG features, including radial processes[9,10]. bRGs are also present in other species, including the mouse[10–15]; however, bRGs are greatly expanded in species with large and folded brains, especially humans, and their expansion is thought to underlie the complexity of the human brain[1–5,11]. Yet little is known about the molecular pathways that lead to the expansion of bRGs and to neocortical growth and folding.

Defective SHH signaling causes holoprosencephaly, a defect in the separation of the brain hemispheres that mostly results from abnormal patterning. Notably, patients with mild holoprosencephaly often have smaller-than-normal brains at birth, or microcephaly[16], suggesting that mechanisms affecting early patterning also affect neurogenesis and brain size. Indeed, mutations in *SHH* and *PATCHED1*, an SHH receptor gene, were found in patients with microcephaly but without holoprosencephaly[17,18]. In mice, defective Shh signaling causes defective proliferation of IPCs and microcephaly[19]; however, the role of SHH signaling in human neocortical development beyond patterning is unknown.

RESULTS

Elevated Shh signaling induces cortical growth and folding

To study the role of Shh signaling in neocortical development without affecting early patterning, we expressed a constitutively active Smoothened (SmoM2), an activator of Shh signaling, in aRGs and their progenies from embryonic day (E) 13.5 by using a *GFAP* promoter–driven Cre. *GFAP::Cre; Gt(ROSA)26Sor*$^{tm1(Smo/EYFP)Amc}$ (*SmoM2*$^{loxP/+}$) mice (*SmoM2* mutants) had cortices larger than those of controls (**Fig. 1**). Remarkably, *SmoM2* mutants consistently developed folding in the cingulate cortex and showed increased cell density in the upper layers of the cingulate and medial cortices (**Fig. 1b**). *SmoM2* mutants normally expressed layer-specific markers (**Fig. 1c**). The density of deep-layer neurons expressing Tbr1 (Tbr1$^+$) was slightly decreased in *SmoM2* mutants, but Satb2$^+$ upper-layer (layer II and III) neurons in the cingulate and medial cortices were denser in *SmoM2* mutants than in controls (**Fig. 1c**,**e**). Notably, white matter extended into the induced gyri (**Fig. 1b**), suggesting that the upper-layer neurons in the folded area had axonal projections. The Satb2$^+$ neuronal density was unchanged in the laterally located sensory cortex (data not shown), which showed no folding. These results suggest that increased Satb2$^+$ upper-layer neurons induce folding in the cingulate cortex.

Elevated Shh signaling expands bRGs and IPCs

To understand upper-layer neuronal expansion, we examined neural progenitors at E16.5, when mostly upper-layer neurons are generated.

[1]Department of Developmental Neurobiology, St. Jude Children's Research Hospital, Memphis, Tennessee, USA. [2]Division of Brain Tumor Research, St. Jude Children's Research Hospital, Memphis, Tennessee, USA. Correspondence should be addressed to Y.-G.H. (young-goo.han@stjude.org).

Received 21 August 2015; accepted 27 April 2016; published online 23 May 2016; corrected after print 28 June 2016; doi:10.1038/nn.4307

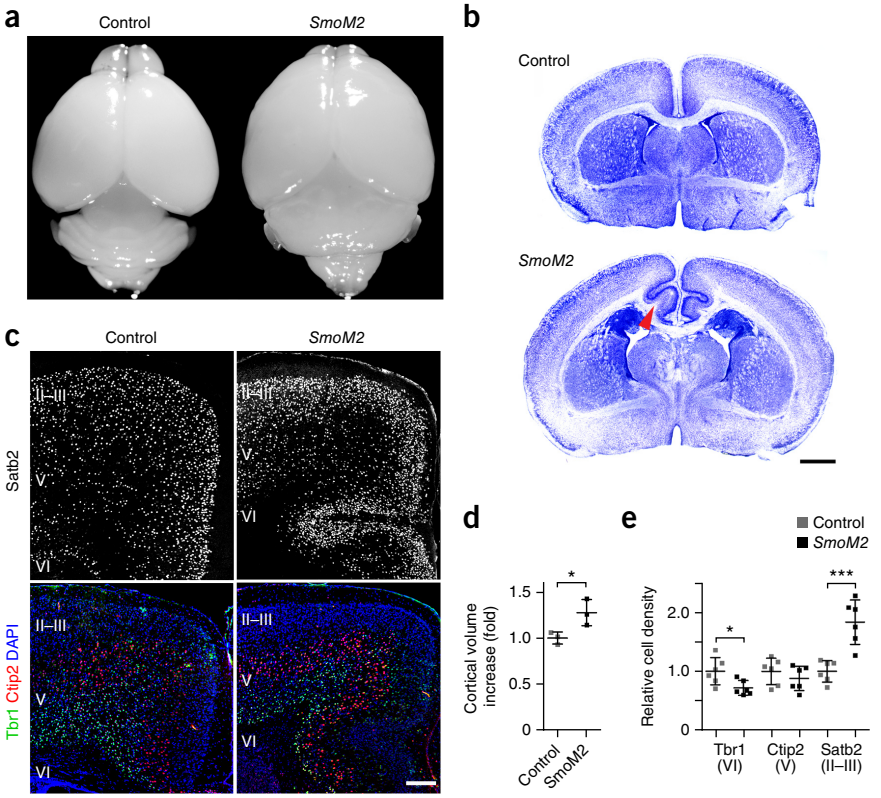

Figure 1 *SmoM2* induces neocortical expansion and folding. (**a**) Control and *GFAP::Cre; SmoM2*$^{loxP/+}$ (*SmoM2* mutant) brains at P10. (**b**) Nissl staining of control and *SmoM2* brain sections at P7. The arrowhead indicates white matter extended into the induced gyrus. Scale bar, 1 mm. Pictures represent at least 5 repeats. (**c**) Expression of layer-specific markers: Satb2 (layers II–III), Bcl11b (Ctip2, red, layer V), Tbr1 (green, layer VI), and DAPI (blue). Scale bar, 0.2 mm. Pictures represent at least 3 repeats. (**d**) Cortical volume calculated from serial MRI scans of P7 control and *SmoM2* mutants. Results were normalized to fold change compared to controls. Two-tailed unpaired *t*-test, $P = 0.0380$, $n = 3$ mice per group. We assumed normal distribution although the number of samples was too small for normality tests. *F*-test for variance, $P = 0.3510$, $F_{(2,2)} = 4.697$. (**e**) Quantification of cell density in the cingulate and medial cortex. Two-tailed unpaired *t*-test, $P = 0.0006$ (Satb2), $P = 0.3634$ (Ctip2), $P = 0.0250$ (Tbr1); $t_{(10)} = 4.877$ (Satb2), $t_{(10)} = 0.9522$ (Ctip2), $t_{(10)} = 2.635$ (Tbr1); $n = 6$ brain slices from 3 mice per group. All data passed Kolmogorov–Smirnov (KS) test for normality ($P > 0.1$) and *F*-test for variance: $P = 4.255$ (Satb2), $P = 0.8609$ (Ctip2), $P = 0.2070$ (Tbr1); $F_{(5,5)} = 0.1380$ (Satb2), $F_{(5,5)} = 1.179$ (Ctip2), $F_{(5,5)} = 3.385$ (Tbr1). $^*P < 0.05$; $^{***}P < 0.001$. Error bars represent s.d.

Consistent with the mitogenic effect of Shh on IPCs[19], IPCs expressing Tbr2 (Eomes) were significantly increased in the *SmoM2* mutants, especially in the SVZ, where most IPCs proliferate (**Fig. 2a**,**c** and **Supplementary Fig. 1**). In controls, Tbr2$^+$ cells spread to the intermediate zone, where newborn neurons maintain Tbr2 (ref. 20). Although the selective expansion of IPCs alone can cause the cortex to grow even larger than in *SmoM2* mutants, such selective expansion does not induce denser upper layers or folding in mice[21], suggesting that additional mechanisms are involved in folding.

The density of Pax6$^+$Tbr2$^-$ aRGs was unchanged in *SmoM2* mutants; however, Pax6$^+$Tbr2$^-$ cells were significantly increased outside the ventricular zone in the *SmoM2* cortex (**Fig. 2a**,**b**). Notably, Pax6$^+$Tbr2$^-$ cells were increased significantly more in the medial than in the dorsal part of the neocortex (1.6-fold; Mann Whitney test; $P = 0.0261$; sum of rank = 89.50, 46.50, $U = 10.50$; standard error = 0.216, 0.096; $n = 8$) reflecting SmoM2 expression along a high-medial to low-lateral gradient in *SmoM2* mutants (**Supplementary Fig. 1c**). The Pax6$^+$Tbr2$^-$ cells outside the ventricular zone also expressed Sox2 (**Supplementary Fig. 2a**), a transcription factor expressed by radial glia. The expression pattern (Pax6$^+$Sox2$^+$Tbr2$^-$) and location of these cells were reminiscent of those of bRGs. Indeed, most Sox2$^+$ cells outside the ventricular zone had processes that were positive for the radial glia markers RC2 and Glast, confirming their bRG identity (**Supplementary Fig. 2a**). In *SmoM2* mutants, bRGs showed diverse morphology, with basal, apical, or bipolar processes oriented radially or tangentially, similar to bRGs in monkeys and ferrets[22,23], and some had a growth cone–like structure, as in human and ferret bRGs[23] (**Supplementary Fig. 2a**).

To test whether SmoM2 increased bRGs cell-autonomously, we induced sparse recombination and labeled the recombined cells with tdTomato in *GFAP::CreER; SmoM2*$^{loxP/+}$*; tdTomato*$^{loxP/+}$ mice by injecting tamoxifen at E13.5 (**Fig. 2d**,**e**). At E16.5, tdTomato$^+$ bRGs were significantly increased in *GFAP::CreER; SmoM2*$^{loxP/+}$*; tdTomato*$^{loxP/+}$ mice compared to controls, indicating cell-autonomous functioning of SmoM2 (**Fig. 2d–f**). As in monkeys[22], bRGs showed diverse morphology, with bipolar bRGs being the most abundant (**Supplementary Fig. 2b**). Thus, SmoM2 cell-autonomously increased bRGs that resembled those in gyrencephalic species.

Elevated Shh signaling keeps bRGs and IPCs in the cell cycle

Manipulating *Trnp1*, PDGFD signaling, or *ARHGAP11B* increases bRGs in mice via delamination of aRGs[24–26]. However, SmoM2 increased the number of bRGs without decreasing that of aRGs (**Fig. 2b**), similar to the initial bRG expansion in humans[1]. Thus, SmoM2 may have raised the number of bRGs by increasing their self-renewal, production, or both. To test if SmoM2 increased self-renewal, we investigated the fraction of self-renewed bRGs remaining in the cell cycle 24 h after the previous S phase by injecting bromodeoxyuridine (BrdU) at E15.5 and 5-ethynyl-2′-deoxyuridine (EdU) at E16.5 1.5 h before collecting embryos (**Fig. 3a**). At E16.5, *SmoM2* mutants showed increased proliferation of IPCs (EdU$^+$) but not of aRGs and bRGs; however, the proportions of bRGs and IPCs remaining in the cell cycle 24 h after the previous S phase (EdU$^+$BrdU$^+$ cells) were significantly higher in *SmoM2* mutants than in controls (**Fig. 3a**,**b**). bRGs migrate basally before dividing; thus, the more they divide and self-renew, the further they move from the ventricular surface[9,12]. Consistent with the increase in BrdU$^+$EdU$^+$ bRGs, bRGs were distributed more basally in *SmoM2* mutants than in controls (**Fig. 3c**), indicating increased self-renewal of bRGs in *SmoM2* mutants.

Elevated Shh signaling shifts aRG division to produce bRGs

Multiple types of bRGs and IPCs, including short neural precursors (also called apical IPCs), are all descendants of aRGs[12,13,22,27,28]. Therefore, we investigated whether aRGs produced more bRGs in

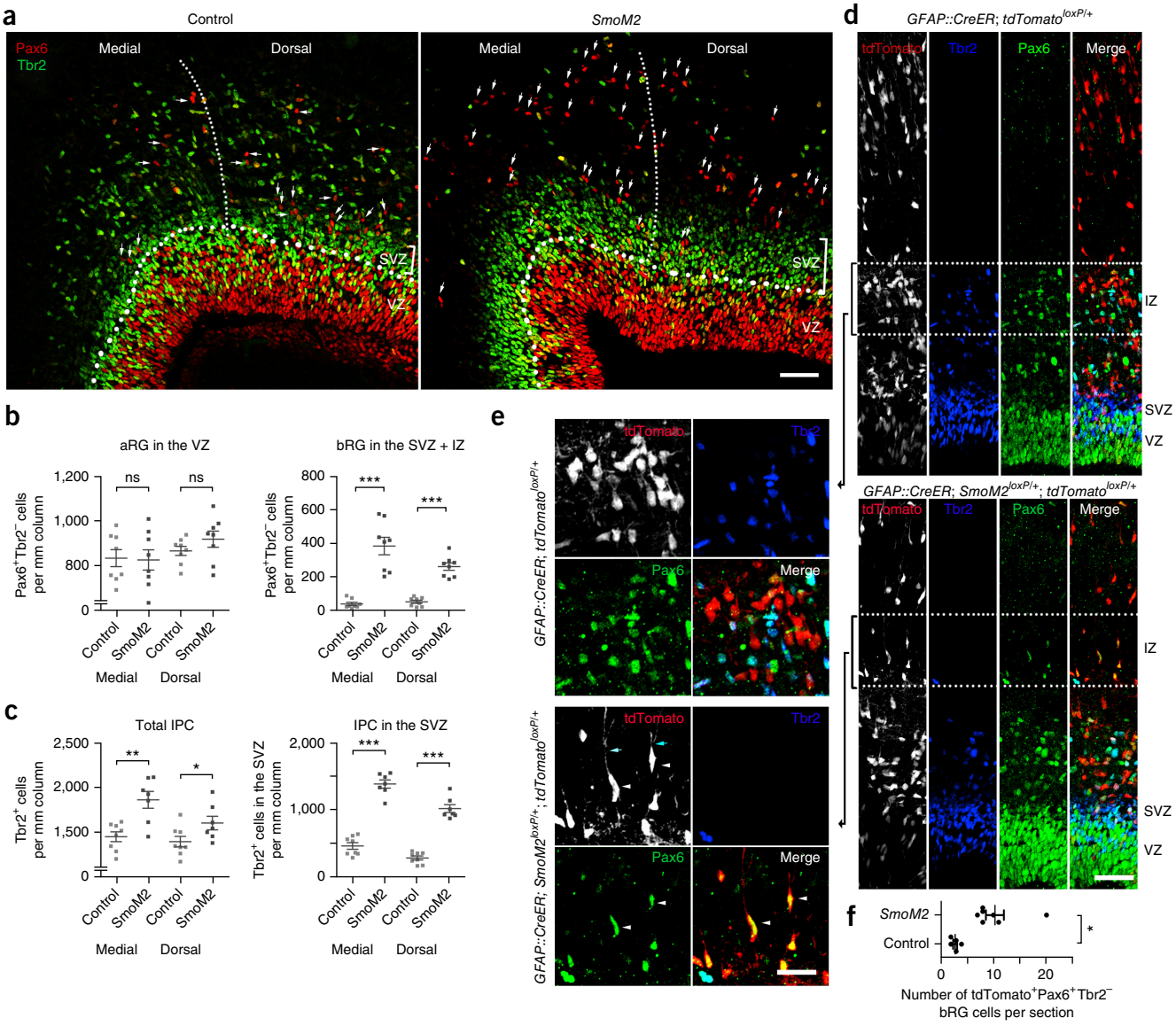

Figure 2 *SmoM2* expands IPCs and bRGs. (**a**) E16.5 cortices labeled for a radial glia marker, Pax6 (red), and an IPC marker, Tbr2 (green). The thin dotted line demarcates the medial (M) and dorsal (D) cortices. The thick dotted line marks the boundary between the ventricular zone (VZ) and SVZ. $Pax6^+Tbr2^-$ cells separated from the VZ by bands of $Tbr2^+$ IPC cells were counted as bRGs (white arrows indicate examples). Pictures represent at least 6 repeats. (**b**) Quantification of $Pax6^+Tbr2^-$ radial glia and (**c**) $Tbr2^+$ IPCs at E16.5. Two-tailed unpaired *t*-test (aRG, IPC, SVZ IPC, equal variance) or two-tailed unpaired *t*-test with Welch's correction (bRG, unequal variance), $P = 0.7888$ (aRG M), $P = 0.2648$ (aRG D), $P = 0.0003$ (bRG M), $P = 0.0001$ (bRG D), $P = 0.0017$ (IPC M), $P = 0.0458$ (IPC D), $P = 0.0000$ (SVZ IPC M), $P = 0$ (SVZ IPC D); $t_{(14)} = 0.2730$ (aRG M), $t_{(14)} = 1.162$ (aRG D), $t_{(7)} = 6.503$ (bRG M), $t_{(9)} = 8.780$ (bRG D), $t_{(13)} = 3.926$ (IPC M), $t_{(13)} = 2.208$ (IPC D), $t_{(13)} = 11.92$ (SVZ IPC M), $t_{(13)} = 11.52$ (SVZ IPC D). All data passed Kolmogorov–Smirnov (KS) testing for normality $P > 0.1$. bRG did not pass an *F*-test for equal variance, $P = 0.6628$ (aRG M), $P = 0.1556$ (aRG D), $P = 0.0003$ (bRG M), $P = 0.0369$ (bRG D), $P = 0.2378$ (IPC M), $P = 0.6396$ (IPC D), $P = 0.7069$ (SVZ IPC M), $P = 0.1388$ (SVZ IPC D); $F_{(7,7)} = 1.408$ (aRG M), $F_{(7,7)} = 3.127$ (aRG D), $F_{(7,7)} = 28.04$ (bRG M), $F_{(7,7)} = 5.603$ (bRG D), $F_{(6,7)} = 2.596$ (IPC M), $F_{(6,7)} = 1.441$ (IPC D), $F_{(6,7)} = 1.336$ (SVZ IPC M), $F_{(6,7)} = 3.350$ (SVZ IPC D), $n = 8$ brain slices from 3 mice per group. (**d**,**e**) E16.5 cortices labeled with Pax6 (green) and Tbr2 (blue) after tamoxifen injection at E13.5. Dotted lines in **d** indicate intermediate zone (IZ) areas enlarged in **e**. (**f**) Quantification of bRGs ($tdTomato^+Pax6^+Tbr2^-$). Two-tailed unpaired *t*-test with Welch's correction, $P = 0.0051$, $t_{(6)} = 4.300$. All data passed Kolmogorov–Smirnov (KS) test for normality, $P > 0.1$. *F*-test for equal variance, $P = 0.0059$, $F_{(6,4)} = 3.350$, $n = 5$ (control) and 7 (*SmoM2*) brain slices from 3 mice per group. $P > 0.05$; $^*P < 0.05$; $^{**}P < 0.01$; $^{***}P < 0.001$; ns, nonsignificant. Scale bars in **a** and **d**, 50 µm; in **e**, 25 µm. Error bars represent s.e.m.

SmoM2 mutants. To compare the direct progenies of aRGs and exclude IPCs and neurons generated from IPCs, we compared cells in the ventricular zone but excluded the SVZ, where IPCs were actively proliferating (**Fig. 3b** and **Supplementary Fig. 3d**). At E15.5, radial glia constituted 49% of the cells in the control ventricular zones and 64% of the cells in the *SmoM2* ventricular zones (**Fig. 3d**,**e** and **Supplementary Fig. 3a**). The percentage of IPCs ($Tbr2^+Pax6^+$ or $Tbr2^+Pax6^-$) and the number of neurons ($TuJ1^+$) were significantly reduced in *SmoM2* ventricular zones (**Fig. 3d**,**e**). Thus, SmoM2-expressing aRGs produced more radial glia at the expense of IPCs and neurons, which may explain the decrease in $Tbr1^+$ neurons (**Fig. 1e**). Despite this, aRGs were not increased at E16.5 in *SmoM2* mutants, whereas bRGs were markedly increased (**Fig. 2b**), suggesting that the additional radial glia in the mutant ventricular zone at E15.5 became bRGs.

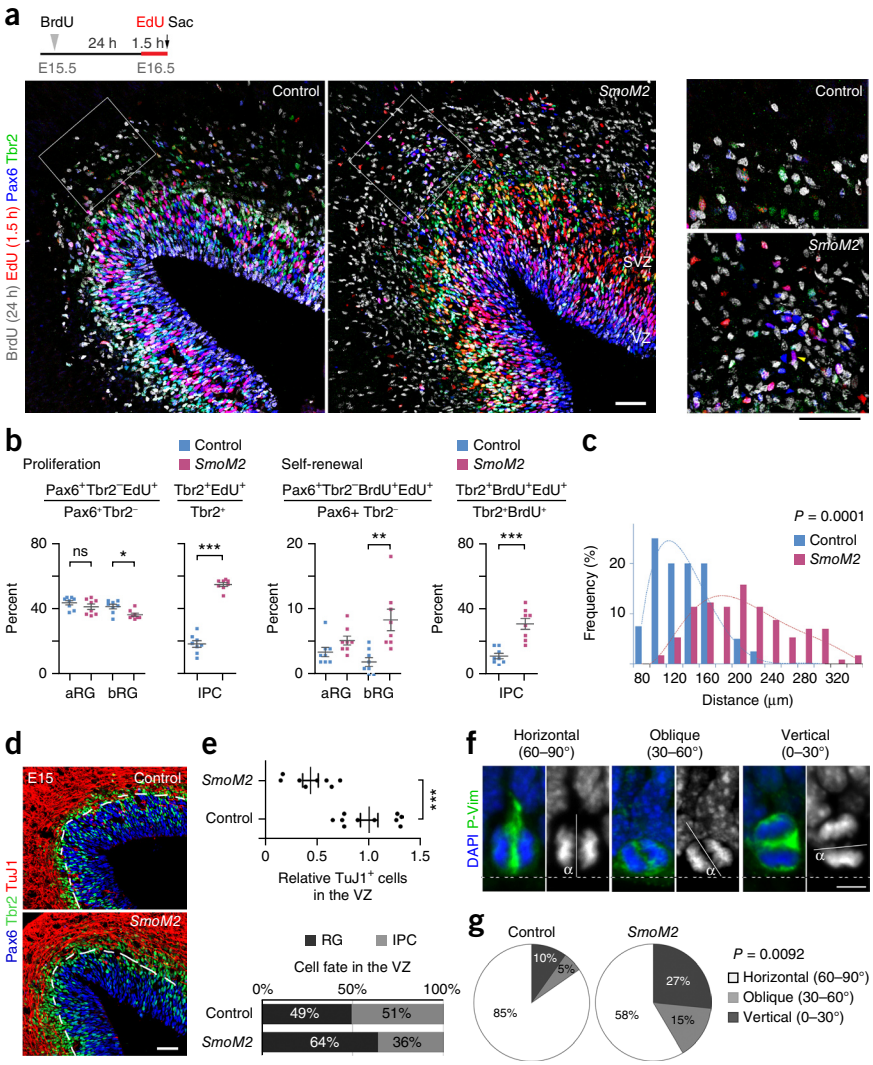

Figure 3 *SmoM2* expands bRGs by increasing their self-renewal and changing the aRG division angle toward bRG production. (**a**) The experimental scheme and E16.5 cortices labeled for Pax6 (blue), Tbr2 (green), BrdU (gray) and EdU (red). The boxed areas are enlarged in the right. Pictures represent at least 3 repeats. (**b**) Proliferation (EdU^+, left) and self-renewal (EdU^+BrdU^+, right) of radial glia and IPCs. All data collected from 8 brain slices from 3 mice per group passed Kolmogorov–Smirnov (KS) test for normality, $P > 0.1$. Two-tailed unpaired *t*-test for proliferation: aRG, $P = 0.2680$, $t_{(14)} = 1.154$; bRG, $P = 0.0103$, $t_{(14)} = 2.960$; IPC, $P = 0.0001$, $t_{(14)} = 15.75$. *F*-test for equal variance: aRG, $P = 0.5533$, $F_{(7,7)} = 1.594$; bRG, $P = 0.3659$, $F_{(7,7)} = 2.045$; IPC, $P = 0.1751$, $F_{(7,7)} = 2.963$. Two-tailed unpaired *t*-test with Welch's correction for self-renewal of bRG: $P = 0.0056$, $t_{(9)} = 3.618$; *F*-test for variance: $P = 0.0274$, $F_{(7,7)} = 6.245$. Two-tailed unpaired *t*-test for self-renewal of IPC: $P = 0.0001$, $t_{(14)} = 5.321$; *F*-test for variance: $P = 0.0869$, $F_{(7,7)} = 4.013$. (**c**) Distribution of the distances of the EdU^+ bRGs from the ventricular surface. Mann-Whitney test, $P = 0.0001$, sum of ranks = 1,392, 10,540, $U = 571.5$, $n = 40$ bRGs for control and 114 bRGs for *SmoM2*. $N = 8$ brain slices from 3 mice per group. (**d**) E15.5 cortices labeled for TuJ1 (red), Pax6 (blue), and Tbr2 (green). (**e**) Numbers of neurons in the ventricular zone (VZ; top) and cell fate (IPC vs. radial glia (RG)) in the VZ (bottom) for the same cortices used in **d**. Pictures represent at least 3 repeats. For relative density of TuJ1 in the VZ, Mann Whitney test, $P = 0.0006$, sum of ranks = 134, 37, $U = 1.000$, $n = 10$ and 8 for control and *SmoM2*, respectively, brain slices from 3 pairs of mice. For ratio of radial glia and IPC in the VZ, Mann Whitney test, $P = 0.0021$, sum of ranks = 28, 77, $U = 0$, $n = 7$ brain slices from 3 mice per group. (**f**,**g**) Mitotic aRGs at E14.5 labeled for phospho-vimentin (P-Vim, green) and DAPI (blue) (**f**) and quantification of the division angle (**g**). We blindly analyzed 101 cells (*SmoM2* mutants) and 71 cells (controls) from 3 pairs of mice. In **f**, α indicates the angle between the apical surface (dotted line) and the plane of division (solid line). The divisions are termed 'horizontal' if $60° < \alpha \leq 90°$, 'oblique' if $30° < \alpha \leq 60°$, and 'vertical' if $0° < \alpha \leq 30°$. Mann Whitney test, $P = 0.0092$, sum of ranks = 6,937, 7,769, $U = 2{,}719$. $P > 0.05$; $^*P < 0.05$; $^{**}P < 0.005$; $^{***}P < 0.001$; ns, nonsignificant. Error bars represent s.e.m. Scale bars in **a** and **d**, 50 μm; **f**, 5 μm.

To investigate the mechanism by which the cell composition changed in the *SmoM2* ventricular zone, we investigated the division angles of aRGs. aRGs dividing on an axis horizontal to the ventricular surface (horizontal division) mostly produce neurons or IPCs, whereas those dividing vertically or obliquely produce bRGs[13,27]. Vertical and oblique divisions were remarkably increased in *SmoM2* mutants, as compared to controls (42% versus 15%) (**Fig. 3f**,**g**). Furthermore, radial glia dividing in the ventricular zone but away from the ventricular surface were significantly increased in *SmoM2* mutants (**Supplementary Fig. 3b**–**d**). Radial glia dividing non-apically in the ventricular zone produce bRGs[23,29] and may also represent bRGs in transit to the SVZ after generation at the ventricular surface; bRGs are also found in the inner SVZ and ventricular zone[11,14,23]. Thus, SmoM2 increased the number of bRGs by shifting aRG division toward bRG production. SmoM2 also greatly increased the number of proliferating IPCs (**Fig. 3b** and **Supplementary Fig. 3b**,**d**), resulting in their expansion in the SVZ despite their decreased production from aRGs (**Fig. 3e**). These results suggest that the expansion of bRGs through increased production and self-renewal, along with an increased number of IPCs, led to neocortical expansion and folding in *SmoM2* mutants.

Fate analysis of progenies from aRGs expressing SMOM2

To confirm that SmoM2 shifted aRG division toward bRG production at the expense of IPCs and neurons, we transduced aRGs sparsely with retroviruses expressing *GFP* either alone or with *SMOM2* (a constitutively active human *SMO*) at E13.5 and examined the fates of GFP^+ cells in transduced clones that had at least two cells. At E15, 46% of clones expressing GFP alone contained only IPCs and/or neurons (IPC/N) without radial glia (IPC/N clones), a further 46% contained one aRG with IPC/N (aRG + IPC/N), and 8% contained two aRGs with or without IPC/N (2aRGs + IPC/N) (**Fig. 4**). Similarly to what we observed in *SmoM2* mutants (**Fig. 3e**), *SMOM2* transduction increased clones containing aRGs to 67% (56% aRG + IPC/N and 11% 2aRG + IPC/N) at the expense of IPC/N clones (33%). Remarkably, by E16, the proportion of aRG-containing clones decreased to the control level (47%), concomitant with a marked increase in the proportion of bRG-containing clones to 23%, which was much higher than that

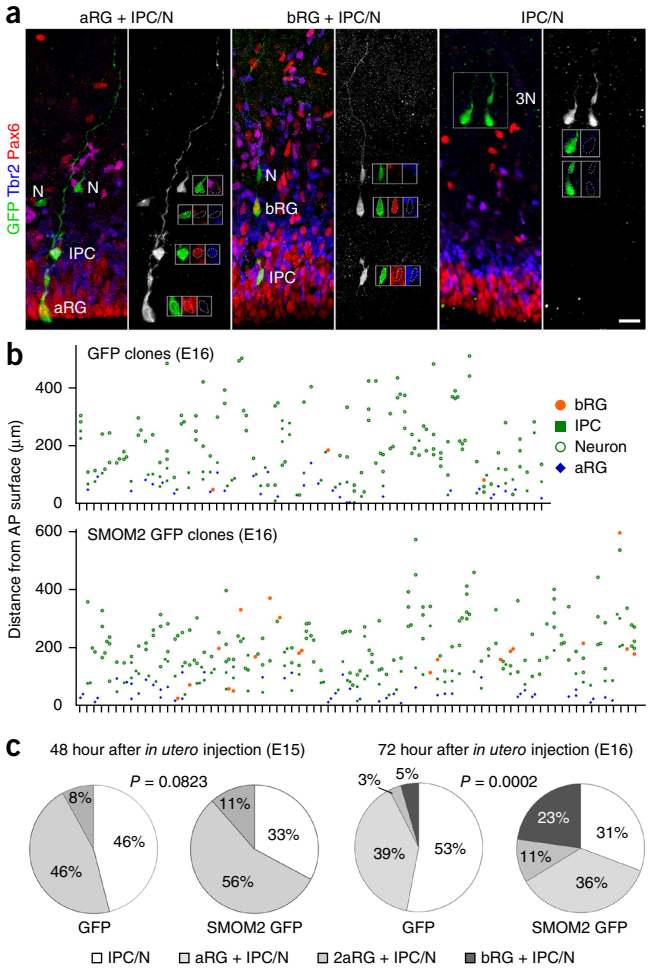

Figure 4 Retrovirus expressing SMOM2 promotes bRG production at the clonal level. (**a**) Micrographs showing examples of different types of clones. Cortices were labeled with GFP (green), Pax6 (red), and Tbr2 (blue) to determine cell fates 48 h (E15) or 72 h (E16) after *in utero* intraventricular injection of GFP or SMOM2 GFP retroviruses at E13. IPC/N clones contained IPCs and/or neurons but no radial glia; aRG + IPC/N clones had one aRG and IPC/N; 2aRG + IPC/N clones had two aRGs with or without IPC/N; and bRG clones had at least one bRG and other cell types. Gray panels include single-channel images for GFP; colored insets show Tbr2 and Pax6 staining for the GFP$^+$ cells. Dotted lines outline the cell bodies of GFP$^+$ cells. Scale bar, 20 μm. (**b**) Composition of individual clones at E16: GFP clones (top) and SMOM2 GFP clones (bottom). Each vertical column of cells above a mark on the *x* axis represents a single clone. (**c**) Distribution of clone types. At E15 (left two charts), we found 23 IPC/N, 23 aRG + IPC/N, and 4 2aRG + IPC/N clones for GFP; and 20 IPC/N, 34 aRG + IPC/N, and 7 2aRG + IPC/N clones for SMOM2 GFP. At E16 (right two charts), we found 35 IPC/N, 26 aRG + IPC/N, 2 2aRG + IPC/N, and 3 bRG clones for GFP; and 31 IPC/N, 36 aRG + IPC/N, 11 2aRG + IPC/N, and 23 bRG clones for SMOM2. Two-sided Fisher's exact test, $P = 0.0823$ at E15 (50 GFP clones, 61 SMOM2 GFP clones), or chi-square test, $P = 0.1659$, $\chi^2_{(2)} = 3.593$ at E15; chi-square test, $P = 0.0002$, $\chi^2_{(2)} = 17.61$ at E16 (66 GFP clones, 101 SMOM2 GFP clones).

observed in control clones (5%). At E16, among clones containing IPCs, the number of IPCs per clone was higher in *SMOM2*-transduced clones than in control clones (1.18 versus 1.36; $P = 0.0158$; Mann Whitney test; sum of ranks = 4,390, 1,938; $U = 1,118$). Together with the results of *SmoM2* mutant analyses, these results indicate that elevated Shh signaling shifts aRG division toward bRG production at the expense of IPCs and neurons and increases the proliferative divisions of IPCs.

SmoM2 induces folding outside the cingulate cortex

In *SmoM2* mutants, folding was present in only the cingulate cortex. As *GFAP::Cre* induces recombination at E13.5 and SmoM2 was expressed in a high-medial to low-lateral gradient in *SmoM2* mutants, we used *Nestin::Cre* (also called *Nes::Cre*) and *Nestin::CreER*, which can induce recombination earlier than E13.5 and did not show such a gradient (**Supplementary Fig. 1c**), to test whether SmoM2 could induce folding outside the cingulate cortex. *Nestin::Cre* induces recombination at E10.5. Only a few *Nestin::Cre; SmoM2$^{loxP/+}$* mutants survived to birth, and these survivors had folding in both the cingulate cortex and other cortical areas (**Supplementary Fig. 4a**). The cortical layering was not disrupted in the folded area (**Supplementary Fig. 4b**). Inducing recombination moderately at E12.5 in *Nestin::CreER; SmoM2$^{loxP/+}$* mutants avoided early lethality and induced folding outside the cingulate cortex (**Supplementary Fig. 4c**). Thus, SmoM2 could induce folding outside the cingulate cortex.

Cortical progenitor specification in *SmoM2* mutants

In contrast to our results, previous studies show that elevating Shh signaling earlier in *Nestin::Cre; Gli3$^{Xt/loxP}$*, *Nestin::Cre; Ptch1$^{loxP/loxP}$*, or *Emx1::Cre; Sufu$^{loxP/loxP}$* mice disrupts the cortical progenitor specification and decreases the number of IPCs and upper-layer neurons[30–32]. The difference in the results is probably due to the different timing and efficiency of Shh signaling activation, because Yabut *et al.* found no specification defects in *GFAP::Cre; Sufu$^{loxP/loxP}$* or GFAP::*Cre; Smo$^{loxP/+}$* mutants[32], overexpression of Shh in the neocortex at E13.5 increased IPCs[33], and we obtained far fewer than expected numbers of *Nestin::Cre; SmoM2$^{loxP/+}$* mutants, suggesting that the few survivors are escapees that may have undergone inefficient recombination. In *Emx1::Cre; Sufu$^{loxP/loxP}$* mice, cortical progenitors ectopically expressed *Dlx2* and *Ascl1* (*Mash1*), which are ventral forebrain progenitor markers[32]; however, their expression was unchanged in our *SmoM2* mutants at E14.5, by which time the aRG division mode had already shifted to produce bRGs (**Supplementary Fig. 5a**). At E16.5, cells expressing Ascl1 and Dlx2 appeared in *SmoM2* mutant cortices (**Supplementary Fig. 5b**); however, the majority of neural progenitors were negative for Ascl1 and Dlx2, unlike those in *Emx1::Cre; Sufu$^{loxP/loxP}$* mice[32]. Notably, a subpopulation of human cortical progenitors express ASCL1, and human bRGs directly produce ASCL1$^+$ cortical progenitors[9]. Thus, the specification of cortical progenitors in our *SmoM2* mutants was largely unaffected and was somewhat similar to that of human cortical progenitors.

SmoM*2* requires cilia and Gli2 to induce neocortical folding

To test whether cilia-dependent canonical Shh signaling was required for folding, we ablated the primary cilia from SmoM2-expressing cells by removing *Kif3a*, an essential ciliogenic gene. The loss of cilia in *GFAP::Cre; SmoM2$^{loxP/+}$; Kif3a$^{loxP/loxP}$* mice blocked neocortical expansion and folding (**Supplementary Fig. 6a**), as did removing Gli2, a transcription factor essential to the Shh-induced transcriptional program, in *GFAP::Cre; SmoM2$^{loxP/+}$; Gli2$^{loxP/loxP}$* mice (data not shown). Therefore, transcriptional regulation through primary cilia and Gli2 was required for SmoM2-driven neocortical expansion and folding.

Loss of *Smo* decreases IPCs, bRGs, and the neocortex

Because elevated Shh signaling expands the bRG population and the neocortex, we investigated whether endogenous Shh signaling affected

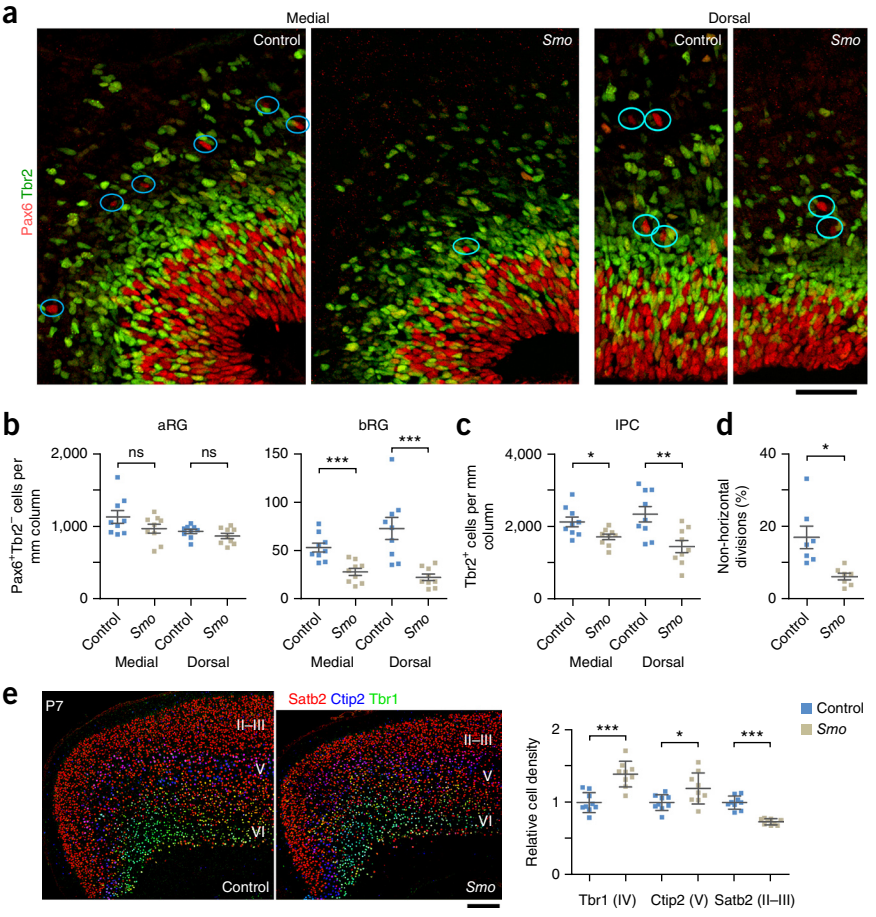

Figure 5 *Smo* is required to expand IPCs, bRGs and upper-layer neurons. (**a**) E16.5 cortices labeled for Pax6 (red) and Tbr2 (green). The circles indicate examples of Pax6^{+}Tbr2^{-} bRGs. Scale bar, 50 µm. We analyzed 9 sections from 3 mice per group. (**b**) Quantification of radial glia. Mann Whitney test; medial aRG, $P = 0.5076$, sum of ranks = 93.50, 77.50, $U = 32.50$; dorsal aRG, $P = 0.3401$, sum of ranks = 97, 74, $U = 29.00$; medial bRG, $P = 0.0005$, sum of ranks = 122, 49, $U = 4.000$; dorsal bRG $P = 0.0002$, sum of ranks = 124, 47, $U = 2.000$. (**c**) Quantification of IPCs. Mann Whitney test; medial IPC, $P = 0.0188$, sum of ranks = 112, 59, $U = 14.00$; dorsal IPC, $P = 0.0078$, sum of ranks = 115, 56, $U = 11.00$. (**d**) Quantification of aRGs dividing non-horizontally ($0° \leq \alpha \leq 60°$). We blindly analyzed 144 cells (*Smo* mutants) and 190 cells (controls) in 7 sections from 3 mice per group. Two-tailed unpaired *t*-test with Welch's correction, $P = 0.0124$, $t_{(7)} = 3.343$; F test for variance, $P = 0.0098$, $F_{(6,6)} = 11.18$. (**e**) Expression and quantification of layer-specific markers: Satb2 (red), Ctip2 (blue) and Tbr1 (green). Scale bar, 0.2 mm. Two-tailed unpaired *t*-test: for Tbr1, $P = 0$, $t_{(16)} = 5.244$; for Ctip2, $P = 0.0271$, $t_{(16)} = 2.432$; for Satb2, $P = 0$, $t_{(11)} = 7.947$. $n = 9$ sections from 3 mice per group. All data passed Kolmogorov–Smirnov (KS) test for normality, $P > 0.1$ and *F*-test for equal variance: $P = 0.4990$, $F_{(8,8)} = 1.642$ (Tbr1), $P = 0.0701$, $F_{(8,8)} = 3.928$ (Ctip2), $P = 0.0418$, $F_{(8,8)} = 4.719$ (Satb2). ns, $P > 0.05$; $^{*}P < 0.05$; $^{**}P < 0.005$; $^{***}P < 0.001$. Error bars represent s.e.m. in **b**–**d** and s.d. in **e**.

the bRG population by deleting *Smo* in *GFAP::Cre; Smo$^{loxP/loxP}$* mice. *Smo* mutants had abnormally small brains (**Supplementary Fig. 6b**) and significantly fewer IPCs and bRGs but not aRGs (**Fig. 5a–c**). Remarkably, the loss of Smo decreased the proportion of aRGs dividing vertically or obliquely (**Fig. 5d**). Consequently, *Smo* mutants had more Tbr1^{+} deep-layer neurons and fewer Satb2^{+} upper-layer neurons than did control mice, the exact opposite of what is found in *SmoM2* mutants (**Fig. 5e** versus **Fig. 1e**). Thus, endogenous Shh signaling was required to expand IPCs, bRGs, upper-layer neurons and the neocortex.

Active SHH signaling in the human fetal neocortex

Despite its critical roles in expanding basal progenitors and the neocortex, Shh signaling is minimally active in the embryonic mouse neocortex. *Gli1*, a faithful marker of strong Shh signaling, is highly expressed in the ganglionic eminence but is undetectable in the embryonic neocortex (**Supplementary Fig. 7a**). Consistently, *lacZ* or *CreER* knocked into the *Gli1* locus labels cells in the ganglionic eminence but not in the neocortex[34]. In contrast, *GLI1* is highly enriched in human aRGs[35]. In the ferret cortex, *Gli1* expression is significantly higher in the region of the ventricular zone that gives rise to the thick oSVZ containing many bRGs than in the ventricular zone region that gives rise to the thin oSVZ containing fewer bRGs[36]. Therefore, strong SHH signaling may contribute to bRG and neocortical expansion in humans. To compare SHH signaling activity in the developing neocortex of humans and mice, we sequenced RNA from the medial or lateral neocortices of E14 mouse embryos and compared *Gli1* levels in our data with *GLI1* levels in human RNA-seq data obtained from BrainSpan (http://brainspan.org/), which also used RNA from macrodissected neocortical tissues. To compare *Gli1* and *GLI1* levels in the two species, we normalized their levels to the expression levels of radial glia markers *SOX2*, *NESTIN* and *PAX6*, which show similar expression patterns in human and mouse radial glia[35]. Notably, *GLI1* and *Gli1* levels correlated positively with bRG numbers in each species. In the human fetal neocortex, *GLI1* levels greatly increased between 9 and 12 postconception weeks (pcw), coincident with bRG expansion, and remained high through mid-gestation, when the oSVZ is the main neurogenic area[9] (**Fig. 6a** and **Supplementary Fig. 8a**). In mice, the *Gli1* level was higher in the lateral cortex than in the medial cortex, consistent with higher numbers of bRGs in the lateral cortex than in the medial cortex[12] (**Fig. 6a**). Notably, the relative *GLI1* levels in human fetuses were higher than were the relative *Gli1* levels in mouse embryos (**Fig. 6a** and **Supplementary Fig. 8b**). Another RNA-seq data set generated from sorted radial glia also showed higher *GLI1* levels in human aRGs[26] (**Supplementary Fig. 8c**). Consistent with the RNA-seq data and in contrast to data from the mouse embryonic neocortex, *in situ* hybridization detected *GLI1* expression in the human neocortical ventricular zone (**Fig. 6b**), as well as in the ganglionic eminence (**Supplementary Fig. 7b**). The transcriptome and *in situ* data suggest potent SHH signaling in the human fetal neocortex.

Next, we investigated the source of SHH in human fetal brains. We detected *SHH* mRNA and SHH protein in the hypothalamic ventricular zone (**Supplementary Fig. 9a**), which could secrete SHH into the ventricle. SHH proteins were consistently highly enriched at the ventricular surface of the neocortex (**Fig. 6c**). In mice, the loss of *Smo* but not of *Shh* in the cortex decreases cortical progenitor proliferation

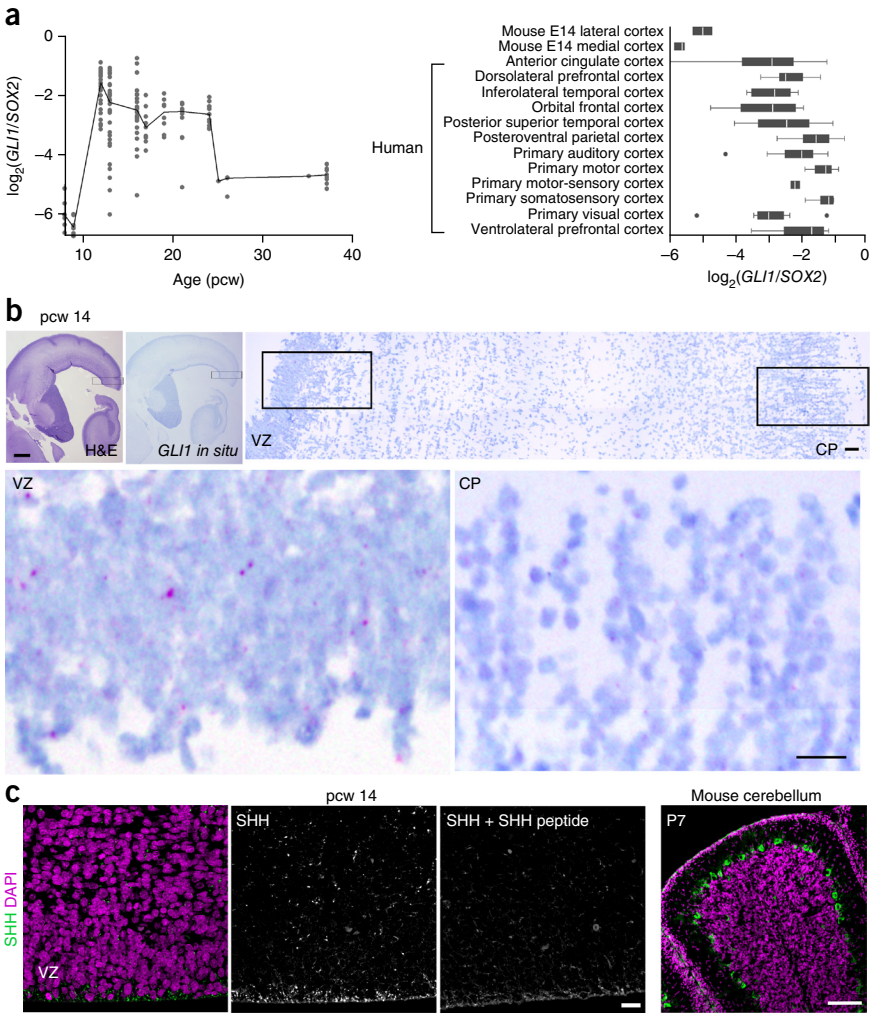

Figure 6 Strong SHH signaling in human aRGs. (**a**) *GLI1* expression during human fetal development (left) and a comparison of *GLI1* and *Gli1* expression levels in developing human and mouse cortices (right). The log *GLI1*/*SOX2* ratio represents $\log_2$(mean FPKM *GLI1*) – $\log_2$(mean FPKM *SOX2*) for humans and $\log_2$(mean FPKM *Gli1*) – $\log_2$(mean FPKM *Sox2*) for mice, where FPKM is fragments per kilobase of transcript per million base pairs mapped. (**b**) Top left: hematoxylin and eosin (H&E) staining and *in situ* hybridization for *GLI1* (purple dots) in the human fetal brain at 14 pcw. The top right panel is an enlargement of the boxed area in the top left panels. Boxed areas in the top right panel are enlarged in the bottom two panels. Scale bars, 1 mm in top left two panels and 50 µm in the enlarged images on the right and bottom. Images represent results from 3 independent tissue samples. (**c**) Left three panels: human fetal brain at 14 pcw stained with anti-SHH antibody (green) and DAPI (purple). Co-incubation with SHH peptide blocks the strong SHH staining at the ventricular surface. This anti-SHH antibody specifically stained Purkinje cells in the mouse cerebellum (right panel), which express Shh. Scale bars, 20 µm in human brain panels and 200 µm in mouse panel. Each figure represents at least 3 repeats on two different tissue samples.

at E15.5[19], suggesting that Shh secreted from outside the cortex regulates cortical progenitor proliferation. Consistently, Shh is present in the embryonic cerebrospinal fluid, and transventricularly delivered Shh regulates neural progenitor proliferation in the cerebellar ventricular zone[37].

SMO inhibitor decreases bRGs in human cerebral organoids

To investigate whether SHH signaling regulates the human bRG population, we employed a cerebral organoid model that recapitulates features of the developing human brain[38]. As reported, this model develops well-defined ventricular-zone- and SVZ-like structures and bRG-like cells (**Supplementary Fig. 10a**).

To investigate whether SHH signaling affects human aRG division angles, we treated organoids with either SANT1 (a SMO antagonist) or SAG (a SMO agonist). In contrast to mouse aRGs (**Fig. 3g**) but similarly to human aRGs in slice culture[27], more than half of the aRGs divided obliquely or vertically in the controls (**Fig. 7a**). Remarkably, SANT1 decreased the incidence of oblique and vertical division to 26%, similar to that found in mouse aRGs, and subsequently decreased the number of $PAX6^+TBR2^-$ bRG-like cells outside the ventricular zone, whereas neither effect was seen with SAG (**Fig. 7a**,**b**). This differential efficacy of SANT1 and SAG may reflect high levels of endogenous SHH signaling in the organoids. To test this, we examined the localization of SMO, which concentrates inside primary cilia upon activation[39]. Consistent with our hypothesis, SMO localized to 51% of the primary cilia in control aRGs, and SAG did not increase ciliary SMO localization, whereas SANT1 decreased it to 19% (**Fig. 7c**). Thus, human cerebral organoids exhibited intrinsic SHH signaling, and blocking this decreased oblique and vertical aRG divisions and the number of bRG-like cells. To test if blocking SHH signaling would affect the production of upper-layer neurons in organoids, we labeled a cohort of cells produced during SANT1 or DMSO (control) treatment with 5-chloro-2-deoxyuridine (CldU). The proportion of $CldU^+SATB2^+$ neurons in $SATB2^+$ neurons was significantly decreased by SANT1 treatment (**Supplementary Fig. 10b**). Thus, blocking SHH signaling decreased the number of bRG and the production of $SATB2^+$ upper-layer neurons in organoids.

A recent study identified genes and a signaling pathway (LIFR–STAT3) selectively enriched in human bRGs (ref. 40). We tested whether antibodies against three of the proteins encoded by genes identified in that study (PTPRZ1, TNC and ITGB5) and phospho-STAT3 could preferentially mark bRGs in human cerebral organoids and *SmoM2* mutants, and found that they did not (data not shown).

DISCUSSION

The prevalence of neocortical folding in many mammalian lineages, the presence of bRGs in all the mammalian species examined and the selective expansion of bRGs in species with large and folded brains suggest that the mechanisms to induce bRG expansion and neocortical folding were present in a common ancestor of mammals and were subsequently selectively fortified or inactivated, giving rise to folded or smooth brains[11]. Our data suggest that Shh signaling has been central to the mechanisms underlying the evolutionary expansion of bRGs and neocortical growth and folding. Shh signaling promoted the expansion of mouse and human bRGs. Its activity was strong in human fetal cortex but not in mouse embryonic cortex, and elevating Shh signaling

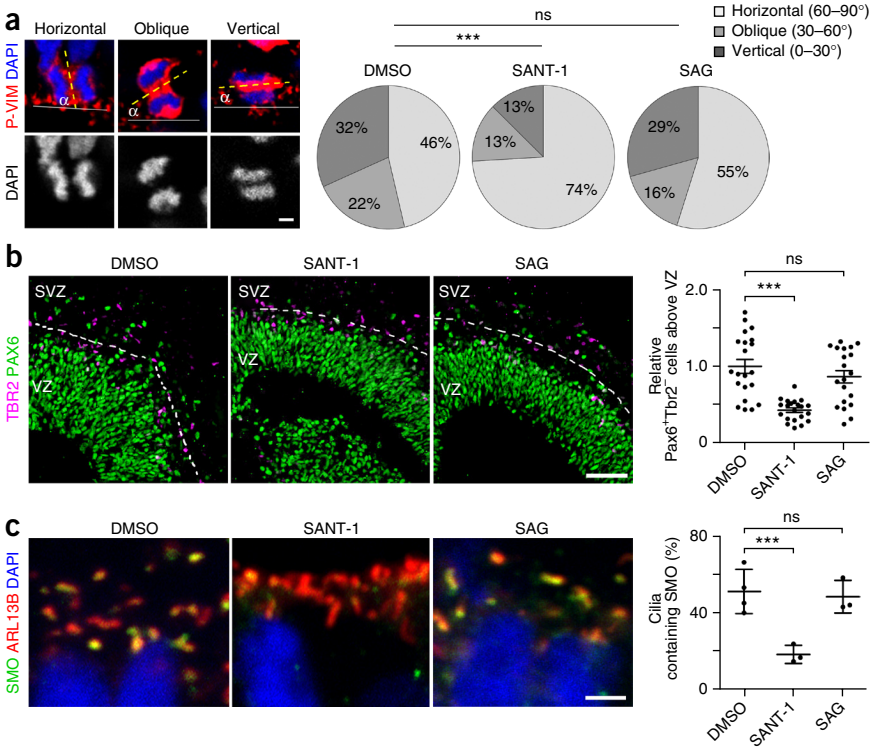

Figure 7 SHH signaling promotes bRG production in human cerebral organoids. (**a**) Examples of horizontal ($60° < \alpha \leq 90°$), oblique ($30° < \alpha \leq 60°$) and vertical ($0° \leq \alpha \leq 30°$) divisions of aRGs in cerebral organoids stained with phospho-vimentin (P-VIM, red) and DAPI (blue) and quantification of the division angles. We blindly analyzed 123 (DMSO), 133 (SAG) and 135 (SANT-1) cells from 15 organoids per group from 3 independent experiments. Mann Whitney test, DMSO vs. SANT-1, $P = 0.0007$, sum of ranks = 14,080, 19,590, $U = 6{,}330$; DMSO vs. SAG, $P = 0.2681$, sum of ranks = 15,336, 17,817, $U = 7{,}586$. Scale bar, 5 µm (**b**) Human cerebral organoids labeled for PAX6 (green) and TBR2 (purple) and quantification of bRGs ($PAX6^{+}TBR2^{-}$ cells separated from dense $PAX6^{+}$ cells by stretches of $TBR2^{+}$ cells that are indicated by dotted lines). We analyzed 21 (DMSO), 20 (SAG) and 21 (SANT-1) VZ and SVZ structures from 11 (DMSO), 13 (SAG) and 15 (SANT-1) organoids from 3 independent experiments. Mann Whitney test, DMSO vs. SANT-1, $P = 0$, sum of ranks = 627.5, 275.5, $U = 44.50$; DMSO vs. SAG, $P = 0.2565$, sum of ranks = 485, 376, $U = 166.0$. Scale bar, 50 µm. (**c**) Apical surfaces of aRGs in organoids labeled for cilia markers (ARL13B, red), SMO (green) and DAPI (blue) and quantification of cilia containing SMO. Scale bar, 2 µm. We examined 294 (DMSO), 292 (SANT-1) and 400 (SAG) cilia from 4 (DMSO), 3 (SANT-1) 3 (SAG) organoids from two independent experiments, of which 145 (DMSO), 53 (SANT-1) and 190 (SAG) cilia contained SMO. Two sided Fisher's exact test, $P = 0.0001$ (DMSO vs. SANT-1), $P = 0.6454$ (DMSO vs. SAG). ns, $P > 0.05$; $^{*}P < 0.01$; $^{***}P < 0.001$. Error bars represent s.e.m. in **b** and s.d. in **c**.

was sufficient to expand bRGs and induce neocortical folding in mice. Importantly, elevating Shh signaling increased the numbers of IPCs as well as bRGs. The expansion of both cell types probably contributes to the neocortical folding in *SmoM2* mutants. The expansion of either progenitor in isolation is insufficient to induce folding[21,41], whereas knockdown of *Trnp1* or overexpression of *ARHGAP11B* induces folding after expanding both IPCs and bRGs[24,26].

Shh signaling expanded bRGs and IPCs through distinct mechanisms. Shh signaling promoted the initial generation and self-renewal of bRGs but did not increase their proliferation rate. In contrast, Shh signaling decreased the numbers of IPCs generated from aRGs but increased their proliferation and the proportion remaining in the cell cycle. Thus, Shh signaling offset the decreased generation of IPCs by promoting their proliferative divisions, leading to their great expansion in the SVZ. Like bRG expansion, the proliferative IPC division is characteristic of primates[9,22]; in rodents, IPCs mainly divide to form two neurons[42–44]. Thus, elevated Shh signaling elicited two developmental characteristics of large and folded brains, bRG expansion and proliferative IPC division, which are proposed to be necessary and sufficient for the evolution of an expanded and folded neocortex[45].

The loss of Shh signaling in *Smo* mutants decreased the numbers of bRGs and IPCs. Previously, we showed that the loss of primary cilia resulted in no apparent defects in cortical development[46]. This seeming discrepancy is probably due to the fact that the loss of cilia results in the loss of both Gli activators and repressors, whereas the loss of Smo causes the loss of Gli activators and an increase in Gli repressors, leading to severer phenotypes than those resulting from the loss of cilia[47–49]. In the developing mouse neocortex, where Shh signaling activity is relatively weak, the loss of Gli activators in cilia mutants may be compensated for by the concomitant loss of Gli repressors. In contrast, the loss of Smo will result in the loss of activators and an increase in repressors, resulting in a pronounced decrease in signaling activity and in defective corticogenesis. We found strong SHH signaling activity in the human fetal cortex; thus, the loss of cilia and the resulting loss of Gli activators may strongly affect human corticogenesis. Notably, many of the genes mutated in congenital microcephaly are essential for the formation and function of centrioles and their associated structures, including cilia[50]. Our findings suggest that defective SHH signaling contributes to congenital microcephaly.

In *SmoM2* mutants, folding occurred in the cingulate cortex, medial to the area that showed the greatest increase in bRGs (the dorsomedial corner of the cortex). Similarly, *Trnp1* knockdown or *ARHGAP11B* overexpression accomplished by *in utero* electroporation induced folding mostly in the cortex medial to the electroporated area that showed an increased number of bRGs[24,26]. It is unclear why the folding occurred preferentially in parts medial to the area with an increased number of bRGs. Neurogenesis proceeds from lateral to medial in mouse cortex. This lateral-to-medial gradient of formation and differentiation of neuronal layers may make those parts medial to the area interrupted by the increase in bRGs and neurons more amenable to structural changes than lateral parts. The physical constraint imposed by the corpus callosum to limit lateral expansion of increased neurons may also have contributed to folding in the cingulate cortex in *SmoM2* mutants.

Conserved genes including *Ccnd1*, *Cdk4*, *Trnp1*, *PDGFD* and *Pax6* and human-specific genes including *ARHGAP11B* may have contributed to the evolutionary expansion and folding of the mammalian neocortex[21,24–26,41]. Shh signaling probably interacts with these and other unidentified genes to generate the complex and large mammalian neocortex. The *SmoM2* mutant, a transgenic mouse model that expands both bRGs and IPCs and consistently develops folding in a defined cortical area, will be important in deciphering these interactions and the mechanisms underlying neocortical development and evolution.

METHODS

Methods and any associated references are available in the online version of the paper.

Accession codes. Gene Expression Omnibus: GSE80958.

Note: Any Supplementary Information and Source Data files are available in the online version of the paper.

ACKNOWLEDGMENTS

We thank S. Baker at St. Jude Children's Research Hospital for the *GFAP::CreER* and *Nestin::CreER* mice; L.S. Goldstein at the University of California San Diego for the *Kif3a*$^{loxP/loxP}$ mice; M.E. Hatley at St. Jude Children's Research hospital for the pBABE-GFP (originally a gift from William Hahn) and pBABE-SmoM2 vectors; J.L. Rubenstein and S. Pleasure at the University of California, San Francisco, for the Dlx2 antibody and the protocol for Ascl1 immunostaining, respectively; and D. Finkelstein and J. Peng at St. Jude Children's Research Hospital for help with the RNA-seq analyses and human embryonic stem cell culture, respectively. Human tissue was obtained from the NIH NeuroBioBank Brain at the University of Maryland, Baltimore, MD. We thank the staff of the Cell and Tissue Imaging Center, the Small Animal Imaging Center, the Hartwell Center for Bioinformatics and Biotechnology, and the Veterinary Pathology Core at St. Jude Children's Research Hospital for technical assistance. We thank S. Baker, X. Cao, M. Dyer, and K.A. Laycock for comments on the manuscript. Y.-G.H. is supported by NIH/NCI Cancer Center Core Support grant CA021765 (SJCRH), the Sontag Foundation Distinguished Scientist Award, Whitehall Foundation research grant, and ALSAC.

AUTHOR CONTRIBUTIONS

L.W. and Y.-G.H. designed and performed the experiments and wrote the manuscript. S.H. performed the *in utero* retroviral injections. Y.-G.H. conceived and supervised the study.

COMPETING FINANCIAL INTERESTS

The authors declare no competing financial interests.

1. Lui, J.H., Hansen, D.V. & Kriegstein, A.R. Development and evolution of the human neocortex. *Cell* **146**, 18–36 (2011).
2. Florio, M. & Huttner, W.B. Neural progenitors, neurogenesis and the evolution of the neocortex. *Development* **141**, 2182–2194 (2014).
3. Borrell, V. & Götz, M. Role of radial glial cells in cerebral cortex folding. *Curr. Opin. Neurobiol.* **27**, 39–46 (2014).
4. Sun, T. & Hevner, R.F. Growth and folding of the mammalian cerebral cortex: from molecules to malformations. *Nat. Rev. Neurosci.* **15**, 217–232 (2014).
5. Dehay, C., Kennedy, H. & Kosik, K.S. The outer subventricular zone and primate-specific cortical complexification. *Neuron* **85**, 683–694 (2015).
6. Smart, I.H.M., Dehay, C., Giroud, P., Berland, M. & Kennedy, H. Unique morphological features of the proliferative zones and postmitotic compartments of the neural epithelium giving rise to striate and extrastriate cortex in the monkey. *Cereb. Cortex* **12**, 37–53 (2002).
7. Zecevic, N., Chen, Y. & Filipovic, R. Contributions of cortical subventricular zone to the development of the human cerebral cortex. *J. Comp. Neurol.* **491**, 109–122 (2005).
8. Lukaszewicz, A. *et al.* G1 phase regulation, area-specific cell cycle control, and cytoarchitectonics in the primate cortex. *Neuron* **47**, 353–364 (2005).
9. Hansen, D.V., Lui, J.H., Parker, P.R.L. & Kriegstein, A.R. Neurogenic radial glia in the outer subventricular zone of human neocortex. *Nature* **464**, 554–561 (2010).
10. Fietz, S.A. *et al.* OSVZ progenitors of human and ferret neocortex are epithelial-like and expand by integrin signaling. *Nat. Neurosci.* **13**, 690–699 (2010).
11. Reillo, I., de Juan Romero, C., García-Cabezas, M.Á. & Borrell, V. A role for intermediate radial glia in the tangential expansion of the mammalian cerebral cortex. *Cereb. Cortex* **21**, 1674–1694 (2011).
12. Wang, X., Tsai, J.-W., LaMonica, B. & Kriegstein, A.R. A new subtype of progenitor cell in the mouse embryonic neocortex. *Nat. Neurosci.* **14**, 555–561 (2011).
13. Shitamukai, A., Konno, D. & Matsuzaki, F. Oblique radial glial divisions in the developing mouse neocortex induce self-renewing progenitors outside the germinal zone that resemble primate outer subventricular zone progenitors. *J. Neurosci.* **31**, 3683–3695 (2011).
14. García-Moreno, F., Vasistha, N.A., Trevia, N., Bourne, J.A. & Molnár, Z. Compartmentalization of cerebral cortical germinal zones in a lissencephalic primate and gyrencephalic rodent. *Cereb. Cortex* **22**, 482–492 (2012).
15. Martínez-Cerdeño, V. *et al.* Comparative analysis of the subventricular zone in rat, ferret and macaque: evidence for an outer subventricular zone in rodents. *PLoS One* **7**, e30178 (2012).
16. Stashinko, E.E. *et al.* A retrospective survey of perinatal risk factors of 104 living children with holoprosencephaly. *Am. J. Med. Genet.* **128A**, 114–119 (2004).
17. Heussler, H.S., Suri, M., Young, I.D. & Muenke, M. Extreme variability of expression of a Sonic Hedgehog mutation: attention difficulties and holoprosencephaly. *Arch. Dis. Child.* **86**, 293–296 (2002).
18. Derwińska, K. *et al.* PTCH1 duplication in a family with microcephaly and mild developmental delay. *Eur. J. Hum. Genet.* **17**, 267–271 (2009).
19. Komada, M. *et al.* Hedgehog signaling is involved in development of the neocortex. *Development* **135**, 2717–2727 (2008).
20. Englund, C. *et al.* Pax6, Tbr2, and Tbr1 are expressed sequentially by radial glia, intermediate progenitor cells, and postmitotic neurons in developing neocortex. *J. Neurosci.* **25**, 247–251 (2005).
21. Nonaka-Kinoshita, M. *et al.* Regulation of cerebral cortex size and folding by expansion of basal progenitors. *EMBO J.* **32**, 1817–1828 (2013).
22. Betizeau, M. *et al.* Precursor diversity and complexity of lineage relationships in the outer subventricular zone of the primate. *Neuron* **80**, 442–457 (2013).
23. Gertz, C.C., Lui, J.H., LaMonica, B.E., Wang, X. & Kriegstein, A.R. Diverse behaviors of outer radial glia in developing ferret and human cortex. *J. Neurosci.* **34**, 2559–2570 (2014).
24. Stahl, R. *et al.* Trnp1 regulates expansion and folding of the mammalian cerebral cortex by control of radial glial fate. *Cell* **153**, 535–549 (2013).
25. Lui, J.H. *et al.* Radial glia require PDGFD-PDGFRβ signalling in human but not mouse neocortex. *Nature* **515**, 264–268 (2014).
26. Florio, M. *et al.* Human-specific gene ARHGAP11B promotes basal progenitor amplification and neocortex expansion. *Science* **347**, 1465–1470 (2015).
27. LaMonica, B.E., Lui, J.H., Hansen, D.V. & Kriegstein, A.R. Mitotic spindle orientation predicts outer radial glial cell generation in human neocortex. *Nat. Commun.* **4**, 1665 (2013).
28. Gal, J.S. *et al.* Molecular and morphological heterogeneity of neural precursors in the mouse neocortical proliferative zones. *J. Neurosci.* **26**, 1045–1056 (2006).
29. Pilz, G.A. *et al.* Amplification of progenitors in the mammalian telencephalon includes a new radial glial cell type. *Nat. Commun.* **4**, 2125 (2013).
30. Wang, H., Ge, G., Uchida, Y., Luu, B. & Ahn, S. Gli3 is required for maintenance and fate specification of cortical progenitors. *J. Neurosci.* **31**, 6440–6448 (2011).
31. Dave, R.K. *et al.* Sonic hedgehog and notch signaling can cooperate to regulate neurogenic divisions of neocortical progenitors. *PLoS One* **6**, e14680 (2011).
32. Yabut, O.R., Fernández, G., Huynh, T., Yoon, K. & Pleasure, S.J. Suppressor of fused is critical for maintenance of neuronal progenitor identity during corticogenesis. *Cell Rep.* **12**, 2021–2034 (2015).
33. Shikata, Y. *et al.* Ptch1-mediated dosage-dependent action of Shh signaling regulates neural progenitor development at late gestational stages. *Dev. Biol.* **349**, 147–159 (2011).
34. Yu, W., Wang, Y., McDonnell, K., Stephen, D. & Bai, C.B. Patterning of ventral telencephalon requires positive function of Gli transcription factors. *Dev. Biol.* **334**, 264–275 (2009).
35. Johnson, M.B. *et al.* Single-cell analysis reveals transcriptional heterogeneity of neural progenitors in human cortex. *Nat. Neurosci.* **18**, 637–646 (2015).
36. de Juan Romero, C., Bruder, C., Tomasello, U., Sanz-Anquela, J.M. & Borrell, V. Discrete domains of gene expression in germinal layers distinguish the development of gyrencephaly. *EMBO J.* **34**, 1859–1874 (2015).
37. Huang, X. *et al.* Transventricular delivery of Sonic hedgehog is essential to cerebellar ventricular zone development. *Proc. Natl. Acad. Sci. USA* **107**, 8422–8427 (2010).
38. Lancaster, M.A. *et al.* Cerebral organoids model human brain development and microcephaly. *Nature* **501**, 373–379 (2013).
39. Corbit, K.C. *et al.* Vertebrate Smoothened functions at the primary cilium. *Nature* **437**, 1018–1021 (2005).
40. Pollen, A.A. *et al.* Molecular identity of human outer radial glia during cortical development. *Cell* **163**, 55–67 (2015).
41. Wong, F.K. *et al.* Sustained Pax6 expression generates primate-like basal radial glia in developing mouse neocortex. *PLoS Biol.* **13**, e1002217 (2015).
42. Noctor, S.C., Martínez-Cerdeño, V., Ivic, L. & Kriegstein, A.R. Cortical neurons arise in symmetric and asymmetric division zones and migrate through specific phases. *Nat. Neurosci.* **7**, 136–144 (2004).
43. Haubensak, W., Attardo, A., Denk, W. & Huttner, W.B. Neurons arise in the basal neuroepithelium of the early mammalian telencephalon: a major site of neurogenesis. *Proc. Natl. Acad. Sci. USA* **101**, 3196–3201 (2004).
44. Miyata, T. *et al.* Asymmetric production of surface-dividing and non-surface-dividing cortical progenitor cells. *Development* **131**, 3133–3145 (2004).
45. Lewitus, E., Kelava, I., Kalinka, A.T., Tomancak, P. & Huttner, W.B. An adaptive threshold in mammalian neocortical evolution. *PLoS Biol.* **12**, e1002000 (2014).
46. Tong, C.K. *et al.* Primary cilia are required in a unique subpopulation of neural progenitors. *Proc. Natl. Acad. Sci. USA* **111**, 12438–12443 (2014).
47. Han, Y.-G. & Alvarez-Buylla, A. Role of primary cilia in brain development and cancer. *Curr. Opin. Neurobiol.* **20**, 58–67 (2010).
48. Han, Y.-G. *et al.* Hedgehog signaling and primary cilia are required for the formation of adult neural stem cells. *Nat. Neurosci.* **11**, 277–284 (2008).
49. Spassky, N. *et al.* Primary cilia are required for cerebellar development and Shh-dependent expansion of progenitor pool. *Dev. Biol.* **317**, 246–259 (2008).
50. Hu, W.F., Chahrour, M.H. & Walsh, C.A. The diverse genetic landscape of neurodevelopmental disorders. *Annu. Rev. Genomics Hum. Genet.* **15**, 195–213 (2014).

ONLINE METHODS

Mice. We used the following mouse strains: *SmoM2*^{flox} (Jackson Laboratory, JAX stock # 005130), *Smo*^{flox} (JAX stock # 004526), *tdTomato*^{flox} (JAX stock # 007909), *GFAP::Cre* (JAX stock # 004600), *Nestin::Cre* (JAX stock # 003771), *Nestin::CreER*^{T2} (ref. 51), *GFAP::CreER* (ref. 52), and *Kif3a*^{flox} (ref. 53). All mice were maintained in a mixed genetic background. To induce Cre-mediated recombination, we used females (2–6 months) carrying the *loxP*-flanked alleles and males (2–9 months) carrying the Cre alleles for breeding. Timed pregnant CD-1 females were purchased from the Charles River Laboratories. All the mice were maintained on a 12 h dark/light cycle and housed with maximum 5 mice of the same sex per cage. We used both sexes for experiments. All animal procedures were approved by the Institutional Animal Care and Use Committee of St Jude Children's Research Hospital.

Human fetal brain samples. Formalin-fixed human fetal brain samples were obtained from the National Institutes of Health NeuroBioBank. The specimens were embedded in paraffin and sectioned coronally at a thickness of 5 µm. The St. Jude Children's Research Hospital Institutional Review Board approved the use of fixed human fetal brain samples.

Thymidine analogs and tamoxifen injection. Solutions of 10 mg/mL bromodeoxyuridine (BrdU) (Sigma B-5002) and 2.5 mg/mL 5-ethynyl-2′-deoxyuridine (EdU) (Invitrogen A10044) were prepared in sterile 0.9% NaCl solution. BrdU (50 µg/g) and EdU (10 µg/g) were injected intraperitoneally into the dam mice at 24 h and 1.5 h, respectively, before euthanasia. Tamoxifen (Sigma T-5648) was dissolved in corn oil (Sigma C-8267) to a concentration of 20 mg/mL by rotation at 65 °C for 1 h. Timed pregnant mice were injected intraperitoneally with tamoxifen at 1.5 mg/40 g at E12.5. For sparse labeling in the tdTomato reporter line, a dose of 0.5 mg/40 g was used.

Histologic processes. Embryonic brains were dissected out, fixed overnight in 4% paraformaldehyde (PFA) in PBS, cryoprotected for 24 h in 30% sucrose in PBS at 4 °C, and embedded in OCT (Sakura Finetek). Tissue blocks were cryosectioned at a thickness of 12 µm and the sections were transferred to glass slides. Postnatal pups were perfused with 4% PFA. Their brains were dissected out, fixed overnight in 4% PFA at 4 °C, embedded in paraffin, and sectioned at a thickness of 5 to 7 µm.

Immunohistochemical staining was performed as described previously[48]. EdU staining was performed using the Click-iT EdU Alexa Fluor® 488 kit in accordance with the manufacturer's instructions. We used the following primary antibodies: anti-Arl13b (Proteintech 17711-1-AP, diluted 1:100), anti-Ascl1 (BD Pharmingen, 1:250; antigen retrieval in 10 mM citric acid buffer pH 6.0 with steam for 10 min), anti-BrdU (Abcam ab1893, 1:500), anti-Ctip2 (Abcam ab18465, 1:500), anti-Dlx2 (ref. 54, a gift from Dr. J. L. Rubenstein, UCSF, 1:1,000), anti-Itgb5 (Abcam ab15459, 1:50), anti-GLAST/EEA1 (Abcam ab416, 1:400), anti-Pax6 (Covance PRB-278P, 1:500; Development Studies Hybridoma Bank AB_528427, 1:200), anti-phospho-histone H3 Ser10 (Abcam 14955, 1:1,000), anti-phospho-Stat3 (Cell Signaling #9145, 1:100), anti-phospho-Vimentin Ser55 (MBL International D076-3, 1:2,000), anti-PTPRZ1 (Sigma HPA015103, 1:250), anti-RC2 (Millipore MAB5740, 1:500), anti-Satb2 (Millipore ABE600, 1:2,000), anti-Shh (Abcam ab73958, 1:100), anti-Smo (Santa Cruz Biotechnology sc166685, 1:50), anti-Sox2 (Y-17) (Santa Cruz Biotechnology sc17320, 1:300), anti-Tbr1 (Millipore AB2261, 1:500), anti-Tbr2 (eBioscience 14-4875-82, 1:250; Abcam ab23345 1:250), anti-Tnc (Abcam ab108930, 1:500), and anti-TuJ1 (Covance MMS435P, 1:1,000). To block anti-SHH staining, we used recombinant human SHH N terminus (R&D 1845-SH-025) at 20-fold molar excess over anti-SHH antibody. The following secondary antibodies were used at 1:400 dilutions and incubated for 2 h at room temperature (20–23 °C) or overnight at 4 °C: Alexa Fluor® 488-conjugated donkey anti-rat IgG (Invitrogen, A-21208), goat anti-chicken IgY (Invitrogen, A-11039), goat anti-mouse IgG/IgM (Invitrogen, A-10684), donkey anti-mouse IgG (Invitrogen, A-21202); Alexa Fluor® 568-conjugated donkey anti-rabbit IgG (Invitrogen, A-10042), donkey anti-mouse IgG (Invitrogen, A-10037) and 647-conjugated donkey anti-goat IgG (Invitrogen, A-21447), donkey anti-rat IgG (Abcam, ab150155), Alexa Fluor® 405-conjugated donkey anti-sheep antibody (Abcam, ab175676), and DyLight™ 405-conjugated donkey anti-mouse IgG (Jackson ImmunoResearch, 715-475-150). Coverslips were mounted on slides with Aqua-Poly/Mount (Polysciences).

Nissl staining was performed with cresyl violet (FD Neurotechnologies) according to the manufacturer's instructions. Before Nissl staining, cryosections were dried overnight at room temperature then defatted in 50% chloroform in ethanol for 24 h.

In situ hybridization (ISH) was performed using an RNAscope® VS Assay (Advanced Cell Diagnostics) with a *GLI1* probe (RNAscope VS Probe - Hs-*GLI1*; Advanced Cell Diagnostics, catalog no. 310996) and an *SHH* probe (RNAscope VS Probe - Hs-*SHH*; Advanced Cell Diagnostics, catalog no. 600956) in accordance with the manufacturer's instructions.

Human cerebral organoids. Cerebral organoids were developed using the protocol of Lancaster *et al.*[38] with minor modifications. Briefly, H9 human embryonic stem cells (hESCs) were obtained from WiCell Research Institute and maintained in mTeSR^{TM}1 medium (Stemcell Technologies) according to the supplier's instructions. To generate embryoid bodies (EBs), hESCs were suspended in low–basic fibroblast growth factor (bFGF) hESC medium consisting of DMEM/F12 (Life Technologies, 11330-032) supplemented with 20% knockout serum replacement (KOSR) (Life Technologies, 10828-028), 3% ES-quality FBS (Life Technologies, 10439-016), 1× GlutaMAX (Life Technologies, 35050-061), 1× MEM-NEAA (Life Technologies, 11140-050), 7 ppm (v/v) β-mercaptoethanol (Life Technologies, 21985-023), 4 ng/mL bFGF (Peprotech, 100-18B), and 50 µM Rho-associated kinase inhibitor (ATCC, ACS-3030) and seeded at 9,000 cells per 150 µL in each well of a 96-well Lipidure®-Coat Plate (Gel Company, LCV96). The medium was changed every other day for 6 to 7 d, omitting the bFGF and ROCK inhibitor after day 4. When the EBs attained a diameter of approximately 500 µm, they were transferred to wells of a Costar® 24-well plate (1 EB per well) (Corning 3473). The EBs were fed every other day with neural induction medium consisting of DMEM/F12 supplemented with 1× N2 supplement (Life Technologies 17502-048), 1× GlutaMAX, 1× MEM-NEAA, and 1 µg/mL heparin for 4 to 5 d until neuroepithelial morphology became evident. The neuroepithelial aggregates were then embedded in a drop of Matrigel (Corning 356234). The embedded aggregates (n = 16) were grown in 6-cm dishes containing 5 mL of differentiation medium (50% DMEM/F12, 50% Neurobasal Medium, 0.5× N2 supplement, 1× B27 without vitamin A (Life Technologies, 12587-010), 0.025% (v/v) human insulin (Sigma, I9278), 3.5 ppm (v/v) β-mercaptoethanol, 1× GlutaMAX, 0.5× MEM-NEAA, and 1× penicillin-streptomycin) with constant shaking at 75 rpm for 4 d; we changed the medium on the second day. Four d after differentiation, the tissue droplets were fed with differentiation medium containing B27 supplement with vitamin A (Life Technologies 17504-044) and incubated for 4.5 weeks at 37 °C in 5% CO_2 with constant rotation at 75 rpm, during which the medium was replenished every 3 d.

To investigate the effects of SHH signaling on bRG generation, cerebral organoids that had been differentiated for 5 weeks (6–10 organoids per well) were treated with 400 nM SAG, 400 nM SANT-1, or DMSO in differentiation medium with vitamin A for 3 d, during which the medium was replenished once 24 h after the initial treatment.

To investigate the effect of SANT1 on upper-layer neuron production, organoids were treated with SANT1 (400 nM) or DMSO for 10 d from 29 to 39 d after differentiation. To label a cohort of neurons produced during treatment, we treated organoids with CldU (3 µg/mL) for 48 h from 35 d to 37 d after differentiation. The organoids were fixed at 64 d after differentiation. We changed the medium every other day; thus, the organoids were treated with fresh SANT1 and DMSO every other day. The organoids were fixed in 4% formaldehyde for 15 min at 4 °C, embedded in 7.5% gelatin, and cryosectioned at a thickness of 20 µm.

Microscopy and data analysis. Images were acquired on a Zeiss780 microscope equipped with a Zen module. To quantify the cell number or density, z-stacks of 4 to 5 optical sections at a step size of 1 µm and a tiling of 4 to 6 images acquired using 20× objectives were combined for analysis. We used at least 3 mutant and 3 control brains for each group. Quantification and analysis were carried out using ImageJ, the image-processing module of Zen (Zeiss), and Photoshop (Adobe).

Determination of ventricular zone, SVZ, aRGs, IPCs, bRGs. For all ventricular zone/SVZ analyses, we stained sections for Pax6 (or Sox2) and Tbr2 to demarcate the ventricular zone and the SVZ. We defined the ventricular zone as the area lining the ventricle and containing dense Pax6$^+$ (or Sox2$^+$) Tbr2$^-$ nuclei up to an area where cells uniformly express Tbr2. We defined the SVZ as the second cell-dense area containing uniformly Tbr2$^+$ cells above the ventricular zone and

below a cell-sparse area. We defined the intermediate zone as the cell-sparse area between the SVZ and the cortical plate, the cell-dense area lying beneath the pial surface. We defined aRGs as $Pax6^+$ (or $Sox2^+$) $Tbr2^-$ cells in the ventricular zone and IPCs as cells expressing Tbr2 irrespective of Pax6 or Sox2 expression. We defined bRGs as $Pax6^+$ (or $Sox2^+$) $Tbr2^-$ cells present above the ventricular zone. Only cells that were clearly separated from the zone of $Pax6^+$ cells by dense $Tbr2^+$ cells were considered to be bRGs.

Human organoid analyses. In organoids, we defined the ventricular zone as the area lining the lumen and containing dense $PAX6^+TBR2^-$ cells up to an area where the cells were sparser than in the ventricular zone and formed stretches of $TBR2^+$ cells. In organoids, there were far fewer $TBR2^+$ cells than in mouse brain, but they formed thin but distinct bands above the ventricular zone to form the SVZ. To quantify the bRG cells, we adopted similar criteria to those used for the mouse brain, i.e., $PAX6^+TBR2^-$ cells above the ventricular zone. A thin but continuous line of $TBR2^+$ cells formed the boundary between the ventricular zone and SVZ. We observed little variation in the thickness of the ventricular zone and SVZ between organoids in the same batch of organoids, though the sizes of the lumen varied substantially. For ventricular zone/SVZ analyses, we only imaged the ventricular zone/SVZs that were (1) not obliquely cut, (2) close to the edges of the organoids to ensure adequate drug access, (3) well separated from the neighboring ventricular zone/SVZ and (4) medial parts of the ventricular zone/SVZ structures in serial sections.

Quantification of spindle orientations: To examine the division angles of vRGs, the cells were stained for P-Vim/PH3/DAPI and examined under 40× or 63× oil objectives. Only cells displaying clear mitotic figures and clear separation of the chromosomes by cytoplasm as revealed by P-Vim staining were included in the analysis. The angles of division were measured using ImageJ.

***In utero* intraventricular injection and clonal analysis.** The plasmid vectors pBABE-GFP (originally a gift from William Hahn; Addgene plasmid # 10668) and pBABE-SMOM2 were gifts from M.E. Hatley at St. Jude Children's Research hospital. We inserted *SMOM2* into *EcoR1* and *Sal1* sites of the pBABE GFP vector to make a pBABE SMOM2 GFP vector, where *LTR* drives *SMOM2* expression and *SV40* promoter/enhancer drives *GFP* expression. Replication-incompetent retroviruses were produced from 293T packaging cell lines. For *in utero* intraventricular injection, timed pregnant CD1 female mice (Charles River Laboratories) of gestation stage E13 were used. Using a Nanoject II Auto-Nanoliter injector (Drummond Scientific), approximately 0.5–0.7 µL of retroviral solution premixed with 1% Fast Green dye was delivered into the lateral ventricles of the embryonic brains via a glass pipette that was pre-beveled on a microgrinder (EG 401, NARISHIGE Groups) and had an opening of 2–3 µm. Glass pipette needles used for microinjection were pulled from glass capillaries (3.5-inch Drummond 3-000-203-G/X, Drummond Scientific) by a P30 micropipette puller (Sutter Instrument Company). Dams were used 48 h (E15) or 72 h (E16) after injection. Coronal sections of 50 µm were collected and stained for GFP, Pax6 and Tbr2. Clones that were clearly separated from each other and were entirely included in the 50-µm thickness were imaged on the confocal microscope using *z*-stacks at step sizes of 1 µm. The $GFP^+Pax6^+Tbr2^-$, GFP^+Tbr2^+($Pax6^+$ or $Pax6^-$) and $GFP^+Pax6^-Tbr2^-$ cells were defined as radial glia, IPCs and neurons, respectively. bRGs were determined as $GFP^+Pax6^+Tbr2^-$ cells located above the ventricular zone, or those cells whose processes clearly had no AP surface attachment. Clones with at least two cells were used for analyses. The clones were classified as follows: IPC/N clones that contained IPCs and/or neurons but not radial glia; aRG + IPC/N clones with one aRG and IPC/N; 2aRG + IPC/N clones with two aRGs with or without IPC/N; and bRG clones with at least one bRG and other cell types.

Magnetic resonance imaging (MRI). To measure the volume of the neocortex, MRI was performed using a 7-T ClinScan animal MRI scanner (Bruker BioSpin MRI GmbH) equipped with a BGA-12S gradient insert and a two-channel phased-array surface coil. Animals were anesthetized with isoflurane (1–2% in O_2) for the duration of the data acquisition. Turbo spin-echo protocols (TR/TE = 1,900–2,500/39–42 ms) were used to acquire T2-weighted images (sagittal, transverse, and coronal) with a matrix of 320 × 320, a field of view of 25 × 25 mm, and a slice thickness of 0.5 mm.

RNA isolation and sequencing. Total RNA was extracted from dissected medial or lateral cortices of E14.5 embryonic brains using the RNeasy Micro Kit (Qiagen). A sequencing library was prepared using the TruSeq Stranded Total RNA Kit (Illumina) and sequenced with an Illumina HiSeq system. FASTQ sequences were mapped to the mm9 genome and counted with HTSEQ[55] and the gene-level fragments per kilobase of transcript per million (FPKM) values were then computed. Exon junction data were extracted through the in-house RNApeg pipeline (M. Edmonson *et al.*, unpublished data). Statistical analyses and visualizations were performed using Partek Genomics Suite 6.6 and Stata MP/11.2 software.

Cross-species RNA-seq comparisons. We used RNA-seq data from human fetal neocortices (8–37 pcw), obtained from BrainSpan (http://brainspan.org/), to plot *GLI1* expression levels over developmental periods. We used RNA-seq data from early mid-trimester human fetuses at 12–19 pcw to compare the expression levels of *GLI1* in humans and *Gli1* in E14 mouse embryonic cortices. As an independent validation of the relative expression levels of *GLI1* and *Gli1*, we also compared them using RNA-seq data from sorted radial glia from the neocortices of human fetuses and mouse embryos (GSE65000) (ref. 26). Given the diverse sources, species and methods of measurement, only the internally controlled relative expression could reasonably be compared. The FPKM data were log-start transformed using the following equation: $\log_2\text{FPKM} = \log_{10}(\text{FPKM} + 2)/\log_{10}(2)$. This variance-stabilizing transformation minimizes the effect of extremely low numbers in ratios arising from low signal strength or low read count. The resulting log ratios of *GLI1* to the established radial glia marker genes *PAX6*, *NES*, and *SOX2* were plotted by category with Stata MP\11.2.

Quantitative reverse transcription PCR. Total RNA extracted from dissected medial cortices of E14.5 embryonic brains was reverse transcribed by Superscript III reverse transcriptase (Invitrogen). Quantitative PCR was performed on an Applied Biosystems 7900 quantitative PCR instrument using SYBR green. Transcript levels were normalized to the expression levels of *Gapdh*. Primer sequences are as follows:

Ascl1 F: CATCTCCCCCAACTACTCCA;
Ascl1 R: CCAGCAGCTCTTGTTCCTCT;
Dlx2 F: AGCTACGACCTGGGCTACAC;
Dlx2 R: TGGCTTCCCGTTCACTATTC;
Gapdh F: CGTCCCGTAGACAAAATGGT;
Gapdh R: GAATTTGCCGTGAGTGGAGT.

Statistics. Statistical analysis was performed using the GraphPad Prism software. All the statistical analyses were two-tailed. Data analyzed by parametric statistical methods (unpaired *t*-tests) were pre-tested for normality by Kolmogorov-Smirnov (K-S) testing and for equal variance by *F*-tests. For normally distributed data with unequal variance, an unpaired *t*-test with Welch's correction was used. We also used non-parametric analysis including the Mann-Whitney test, chi-square test, and Fisher's exact test. *P* values of less than 0.05 were considered significant. No statistical methods were used to predetermine the sample size, but our sample sizes are similar to those generally employed in the field. The mice were not randomized. The investigators were not blinded to sample identity, except in the analyses of the division angles of mouse and human vRGs. No animal or data points were excluded from analysis.

A **Supplementary Methods Checklist** is available.

Data availability. The data that support the findings of this study are available from the corresponding author upon request.

51. Zhu, G. *et al.* Pten deletion causes mTorc1-dependent ectopic neuroblast differentiation without causing uniform migration defects. *Development* **139**, 3422–3431 (2012).
52. Chow, L.M.L., Zhang, J. & Baker, S.J. Inducible Cre recombinase activity in mouse mature astrocytes and adult neural precursor cells. *Transgenic Res.* **17**, 919–928 (2008).
53. Marszalek, J.R. *et al.* Genetic evidence for selective transport of opsin and arrestin by kinesin-II in mammalian photoreceptors. *Cell* **102**, 175–187 (2000).
54. McKinsey, G.L. *et al.* Dlx1&2-dependent expression of Zfhx1b (Sip1, Zeb2) regulates the fate switch between cortical and striatal interneurons. *Neuron* **77**, 83–98 (2013).
55. Anders, S., Pyl, P.T. & Huber, W. HTSeq–a Python framework to work with high-throughput sequencing data. *Bioinformatics* **31**, 166–169 (2015).

doi:10.1038/nn.4307

Corrigendum: Hedgehog signaling promotes basal progenitor expansion and the growth and folding of the neocortex

Lei Wang, Shirui Hou & Young-Goo Han

Nat. Neurosci. **19, 888–896 (2016); published online 23 May 2016; corrected after print 28 June 2016**

In the version of this article initially published, the units on the *x* axis in Figure 3c were given as mm; the correct units are μm. At the end of the legend to Figure 7, the error bars were described as s.d.; they are actually s.e.m. in **b** and s.d. in **c**. In the third sentence of the Online Methods section on human cerebral organoids, 10% knockout serum replacement, 1% GlutaMAX and 1% MEM-NEAA should have been 20%, 1× and 1×, respectively. In the sixth sentence, 1% N2 supplement, 1% GlutaMAX and 1% MEM-NEAA should each have been 1×. In the eighth sentence, 6-mm dishes should have been 6-cm dishes, 0.5% N2 supplement and 0.5% MEM-NEAA should each have been 0.5×, and 1% B27 without vitamin A, 1% GlutaMAX and 1% penicillin/streptomycin should each have been 1×. In Supplementary Figure 10b, the graph lacked error bars. The errors have been corrected in the HTML and PDF versions of the article.